Simulation of bio-inspired micro-swimmers with varying material composition

L. Offereins*, S. Mohanty, S. Misra

University of Twente, Faculty of Engineering Technology, Drienerlolaan 5, 7522 NB, Enschede, The Netherlands
**corresponding author l.offereins@student.utwente.nl*

ABSTRACT: A simulation of a bio-inspired micro-swimmer excited with traveling soundwaves is presented. Four designs are presented to realize a variation in material composition, inducing acoustic and structural asymmetry in the swimmer to maximize the amount of propulsion. The designs are simulated with the COMSOL Multi-Physics FEM-application. From structural analysis eigenfrequencies and mode shapes of the swimmer are determined and acoustic excitation is shown to induce the same response in the swimmer. In acoustofluidic analysis a perturbation approach is used to decouple first and second order effects. Propulsive force was found to be maximized at eigenfrequency. Future applications of the swimmer include targeted drug delivery and non-invasive surgery.

Key words: micro-robotics, material inhomogeneity, acoustic actuation, acoustofluidics, propulsion

1 INTRODUCTION

Remote actuation of micro-particles by using external means has become an interesting field of study over the last ten years. At small scale volumetric effects become of less importance than surface effects, due to the large surface areas. For micro-particles this leads to a dominance of surface dependent viscosity drag, over bulk inertia forces and therefore regular propulsion methods become ineffective [1]. Propulsion at this scale can be achieved by copying swimming movements of biological swimmers, such as flagellated bacteria, ciliates or sperm cells [2]; or by passively guiding the particles through the environment. Either one of these propulsion methods can be induced with, amongst others, magnetic [3], electric [4] and acoustic fields [5], [6]. A special application of these means of actuation lies in the medical field, where micro-particles can be used for in-vivo applications like localized targeted drug delivery, thereby enhancing accuracy of medication and it could in some cases provide an alternative as a non-invasive surgical treatment [7].

Acoustic actuation could prove to be of interest for the medical field, as multiple uses of soundwaves are biocompatible [8]. Acoustic actuation is possible either by standing wave, as passive guidance, or by traveling wave, by inducing a swimming motion in the particle. For the former an intimate knowledge of the particles environment must be available, such that the standing wave can be optimally constructed to guide the particle along the path, as demonstrated by Nilsson et al. [9]. Establishing a standing wave in in-vivo conditions requires precision and prerequisite knowledge of the environment. Due to the nature of in-vivo applications the domain is relatively complex and largely unknown, therefore standing wave actuation might not prove to be effective. As such knowledge is not required for the construction of a traveling soundwave, this option is more viable. Actuation with traveling soundwaves has already proved effective as demonstrated by Ahmed et al. [6], [10], and Kaynak et al. [11], and this study will make use of this type of actuation as well.

Introducing asymmetry in the particle, either in geometry or with material combination, will lead to a difference in sound propagation through the particle. This will in turn induce a different mechanical response which could lead to a swimming motion in the particle. The question we ask is, whether and how the combination of different materials influences the amount of propulsion achieved. Ahmed et al. have demonstrated that the combination of two materials does alter the behavior of the particle [6]. This paper presents a design based evaluation of propulsive forces acting on an asymmetric micro-particle, referred to as a swimmer, and focuses on how selective material design could lead to enhancement of these forces.

2 METHODOLOGY

Four different designs are employed to study the material influence on propulsion. Figure 1 gives an overview of the designs, which all have a different distribution of two materials. The material with the highest density, indicated in gray in figure 1, is concentrated in the head. The two material and shell designs have an abrupt material transition on the surface the effect of which will be interesting to study in streaming patterns. The two material design is a purely theoretical model, while the shell swimmer is adapted for fabrication with a sputtering technique [12]. The cavity swimmer has a homogeneous surface so any variation in the streaming pattern will not be due to a different interaction between swimmer surface and fluid medium. This model is also suitable for fabrication and can be constructed with either electro-deposition [13], or a relatively new fabrication method called focused electron beam induced deposition [14]. Two contrasting materials are combined to increase the amount of propulsion of the swimmer. This contrast will entail different mechanical behavior and acoustic impedances. Variation in material properties such as stiffness or density should elicit a change in the location of eigenfrequencies and with that a change in the frequency at which maximum propulsion can be achieved. Different acoustic impedances can promote the asymmetry of the swimmer design, which will cause the swimmer to respond to acoustic actuation differently. An acoustically heavy head and lighter, more flexible tail, will decrease the movement of the head and could promote propulsion to results in more straight-lined movements. The swimmer has a length of 300 micron, with an ellipsoid head and a tapered tail.

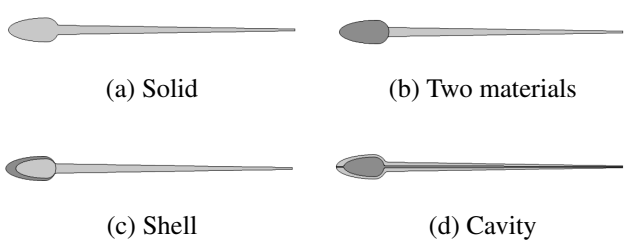

(a) Solid (b) Two materials

(c) Shell (d) Cavity

Fig. 1: Structural designs of the micro-swimmers

The analysis of the situation is broken down into three components, to identify the different aspects that contribute to the behavior of the swimmer. The first component concerns a structural analysis, performed to determine the eigenfrequencies and modes of the swimmer. The second considers an acoustic excitation of a surrounding medium to verify whether it can elicit the same response as a mechanical excitation. And finally, the last component considers the swimmer in a fluidic environment, where it will be exposed to a traveling soundwave.

2.1 Structural Analysis

This study component will show whether it is possible to induce vibrational modes in the design with an harmonic load placed on the swimmer and locate the frequencies at which these modes occur. The deformation of each mode will be evaluated. The eigenfrequencies and mode shapes will provide comparison for excitation with acoustics. The swimmer is modeled with the structural mechanics module. A COMSOL eigenfrequency study is performed to find the eigenfrequencies and their corresponding mode shapes. A harmonic excitation is placed on one side of the tail, while the head is secured with a fixed constraint to prevent rigid body modes. A variation of materials and material combinations will be tested to investigate the different responses of the swimmer.

2.2 Acoustics

Next it will be investigated whether actuation by soundwaves can induce a mechanical response in the swimmer. Eigenfrequencies and mode shapes can be compared with those of the mechanical excitation to search for similarities and dissimilarities. The head of the swimmer will be constrained as to make the situation similar to the purely mechanical excitation. The environment of the swimmer is modeled with a pressure acoustics domain which is excited by a plane wave radiation to simulate the acoustic excitation.
To account for any dampening effects of the soundwave due to viscous properties of the surrounding medium, another simulation will be performed were the pressure acoustics module will be replaced with a thermo-viscous acoustics module. Though the environment of the swimmer is modeled with the properties of water, fluid behavior is not yet taken into account. The fluid will be excited with a soundwave modeled as an initial velocity: $1[nm] * i * \omega_{ta} * t$ in which ω_{ta} is the changing angular velocity and t the time. To evaluate the mechanical response, the elastic strain energy is measured with respect to the frequency. A higher value of the eigenfrequency is now

expected in comparison with the previous step due to the dampening effect.

2.3 Acoustofluidics

Lastly the swimmer is modeled within an environment where the physics of the fluid, acoustic and structural interfaces is combined. This section describes how the fluid response to an acoustic excitation can be modeled with a numerical approximation approach. This governs the acoustofluidic interaction in the medium and specifically in the area around the swimmer, allowing an estimation of the forces the fluid will exert on the swimmer. The designs will have different pressure distributions along their surfaces which cause a variation in the streaming patterns around the swimmer. These distinct streaming patterns will cause a change in the magnitude and direction of the forces acting on the swimmer.

2.3.a Governing Equations

The fluidic environment of the swimmer is modeled as a compressible viscous fluid with the corresponding continuity and Navier-Stokes equations:

$$\frac{\partial \rho}{\partial t} + \nabla \cdot (\rho \mathbf{v}) = 0 \tag{1}$$

$$\begin{aligned}\frac{\partial}{\partial t}(\rho \mathbf{v}) + \rho(\mathbf{v} \cdot \nabla)\mathbf{v} = -\nabla p + \mu \nabla^2 \mathbf{v} \\ +(\mu_b + \frac{1}{3}\mu)\nabla(\nabla \cdot \mathbf{v})\end{aligned} \tag{2}$$

In which ρ is the density of the fluid, $\boldsymbol{v}$ the fluid velocity, p the fluid pressure and μ and μ_b the dynamic and bulk viscosities.

A typical approach to find the solutions for these computationally heavy equations is Nyborgs perturbation theory, as demonstrated by for instance Bruus [15]. Here the velocity, pressure and density fields are assumed to be of the following form:

$$\begin{aligned}\rho &= \rho_0 + \rho_1 + \rho_2 \\ p &= p_0 + p_1 + p_2 \\ \mathbf{v} &= \mathbf{v}_1 + \mathbf{v}_2\end{aligned} \tag{3}$$

The subscript 0, 1 and 2 indicate the quiescent, first order and second order terms. The first order terms have a harmonic time dependence and are caused by the acoustic perturbations. The second order terms arise due to acoustic streaming effects, originating from the non-linear terms in the Navier-Stokes equation. When equations 1 and 2 are linearized, the first and second order fields can be separately solved for and the combined solution will be the approximate total solution.

Due to the harmonic time dependence the first order fields can be assumed to be of the form $e^{i\omega t}$. The linearized first order continuity and Navier-Stokes equations then become:

$$\frac{\partial \rho_1}{\partial t} = -\rho_0 \nabla \cdot \mathbf{v}_1 \tag{4}$$

$$\rho_0 \frac{\partial \mathbf{v}_1}{\partial t} = -\nabla p_1 + \mu \nabla^2 \mathbf{v}_1 + (\mu_b + \frac{1}{3}\mu)\nabla(\nabla \cdot \mathbf{v}_1) \tag{5}$$

The non-linear terms, $-\nabla \cdot (p_1 \mathbf{v}_1)$ and $\rho_1(\partial \mathbf{v}_1/\partial t) + \rho_0(\mathbf{v}_1 \cdot \nabla)\mathbf{v}_1$ will be used as source terms for the second order equations.

Using the second order perturbation described in equation 3 the following second order continuity and Navier-Stokes equations are obtained:

$$\frac{\partial \rho_2}{\partial t} = -\rho_0 \nabla \cdot \mathbf{v}_2 - \nabla \cdot (\rho_1 \mathbf{v}_1) \tag{6}$$

$$\begin{aligned}\rho_0 \frac{\partial \mathbf{v}_2}{\partial t} = -\nabla p_2 + \mu \nabla^2 \mathbf{v}_2 + (\mu_b + \frac{1}{3}\mu)\nabla(\nabla \cdot \mathbf{v}_2) \\ -\rho_1 \frac{\partial \mathbf{v}_1}{\partial t} - \rho_0(\mathbf{v}_1 \cdot \nabla)\mathbf{v}_1\end{aligned} \tag{7}$$

Ordinarily the second order fields would be negligible with respect to the first order fields. Yet since the first order fields have a harmonic time dependence and the second order streaming effects are steady, solutions to both equations are at different time-scales. Over time the second order solutions will have a significant contribution to the total problem and can therefore not be neglected. To solve for the second order equations an average over the time of one oscillation period can be taken. The contribution of the first order solution to the second order equations is then made by the terms that don't average out over the oscillation period. The time-averaged continuity and Navier-Stokes equations for the second order become:

$$\rho_0 \nabla \cdot \langle \mathbf{v}_2 \rangle = -\nabla \cdot \langle \rho_1 \mathbf{v}_1 \rangle \tag{8}$$

$$\mu\nabla^2\langle\mathbf{v}_2\rangle + (\mu_b + \frac{1}{3}\mu)\nabla(\nabla\cdot\langle\mathbf{v}_2\rangle) - \nabla p_2 = \left\langle \rho_1 \frac{\partial \mathbf{v}_1}{\partial t} \right\rangle + \rho_0\langle(\mathbf{v}_1\cdot\nabla)\mathbf{v}_1\rangle \quad (9)$$

In which the angled brackets denote a time-average over one oscillation period.

The forces acting on the swimmer can be divided into three categories: the acoustic radiation force, the Stokes drag and the force due to the harmonic first order fields. The combined force is presented as follows:

$$\left\langle \int_{S(t)} (\bar{\sigma_1}\cdot\mathbf{n})\, dS \right\rangle + \int_{S_0} (\langle\bar{\sigma_2}\rangle\cdot\mathbf{n})\, dS \quad (10)$$

In which $\bar{\sigma_1}$ and $\bar{\sigma_2}$ are respectively the first and second order stress tensors, $\mathbf{n}$ the outward pointing unit normal vector of the surface, $S(t)$ the surface of the swimmer that changes with time and S_0 the time-invariant swimmer surface, as steady streaming is assumed for the second order solution. The first component of the force contains the influence of the first order solution, this force can be computed by rewriting the integral using the Leibniz Reynolds Transport Theorem [16], as presented in the following equation

$$\left\langle \int_{S(t)} (\bar{\sigma_1}\cdot\mathbf{n})\, dS \right\rangle = -\left\langle \int_{S(t)} \rho_0\mathbf{v}_1\mathbf{v}_1\cdot\mathbf{n}\, dS \right\rangle \quad (11)$$

This force will be referred to as the LRTT force. The second part of equation 10 contains the contribution of the acoustic radiation force, described by the time-averaged second order pressure $\langle p_2\rangle$, and the Stokes drag force, which is due to the time-averaged second order streaming velocity $\rangle\mathbf{v}_2\langle$.

2.3.b Modeling

The acoustofluidic situation can be separated into two timescales. The first containing the acoustic perturbation and the second the streaming effects. To solve for the first timescale the structural mechanics module and the thermo-viscous acoustics module of COMSOL are coupled and the variables are computed within the frequency domain. The model is meshed with a grid that changes with the magnitude of the frequency and the excitation soundwave is scaled with respect to frequency and domain size. The results from this study are then used as input for the second order equations, which deliver the streaming patterns and the magnitude of the propulsive forces. The laminar flow module of COMSOL is utilized and a stationary study is performed. The computations in the frequency domain are performed in an environment bounded by perfectly matched layers (PMLs). These prevent any reflection of the acoustic wave on the boundary, thereby imitating an infinite domain. To find expressions for the acoustic radiation force and the Stokes drag the second order pressure field and the viscous stress variables of the COMSOL environment will be used. Simulation parameters and scaling factors can be found in appendix A.

The situation will be analyzed in two steps. First, the designs will be investigated at their eigenfrequencies. The amount of propulsion is expected to be higher at these frequencies and any effect of material inhomogeneity can be better observed [6]. Then simulations will be run for some frequencies across the suitable frequency range of 50 till 150 kHz [15]. At 50, 75, 100 and 150 kHz simulations will be performed and the collected data will be force quantities, namely the acoustic radiation force, the Stokes drag and the LRTT force; elastic strain energy and streaming patterns. A simulation will also be run for 10kHz, this frequency falls outside of the range of suitable frequencies and will serve as comparison level.

3 RESULTS

3.1 Structural Analysis

A variation of materials was selected to provide contrasting mechanical responses from the swimmers. SU8, PDMS, iron and titanium were used in the simulations. SU8, an expoxy photoresist, is a well-known material for micro-electromechanical systems (MEMS) and has good biocompatibility [17]. PDMS is a silicon-based polymer which is often used in MEMS because it enables the construction of shapes with a precision up to 0.1 micron [18]. Iron is used to represent a typical metal, and is applicable for deposition. Titanium is added to investigate whether different metals show large differences in the swimmers response. Material properties are used as provided by COMSOL. The first three eigenfrequencies obtained for all models are presented in the table below. The table shows that eigenfrequencies of the shell designs closely resemble those of the solid designs, with the corresponding primary material component. The cavity model is distinct from the other models with higher eigenfrequencies.

Table 1: First three eigenfrequencies of all swimmer designs, the primary component is named first in the designs constructed of two materials

Design	Materials	Eigenfrequencies (kHz)		
		1st	2nd	3rd
solid	PDMS	.964	3.55	8.32
	Fe	164	604	1414
	SU8	51.8	191	447
	Ti	158	529	1364
mat2	PDMS-SU8	.982	3.62	8.49
	PDMS-Fe	.982	3.62	8.49
	PDMS-Ti	.981	3.62	8.49
	SU8-Fe	52.8	195	457
	SU8-Ti	52.7	195	456
cavity	PDMS-SU8	6.05	27.1	68.4
	PDMS-Fe	26.6	123	309
	PDMS-Ti	24.1	111	280
	SU8-Fe	40.7	173	432
	SU8-Ti	44.6	182	446
shell	PDMS-SU8	.970	3.58	8.38
	PDMS-Fe	.971	3.58	8.38
	PDMS-Ti	.971	3.58	8.38
	SU8-Fe	52.1	192	450
	SU8-Ti	52.0	192	450

The mode shapes of the swimmer for each eigenfrequency remain the same across all designs and can be found in figure 2.

3.2 Acoustics

Excitation with soundwaves proved to be able to induce a mechanical response in the swimmer. At its eigenfrequencies the swimmer assumes the same shapes as with mechanical excitation. The eigenfrequencies occur at much lower frequencies than before, on average 0.25 times the frequency found in the structural analysis. Since the responses of swimmers constructed with titanium or iron still remained similar, it was decided to choose only one of these metals in further simulations. As the iron swimmers have slightly higher eigenfrequencies than the titanium ones, iron was selected.

Within the thermo-viscous module frequency responses were obtained from a range between 10 kHz and 500 kHz, simulations were performed at steps of 1 kHz. Figure 3 shows the response of all swimmer designs and for PDMS-Fe and PDMS-SU8 combinations. Simulations were performed for all designs with a SU8 and iron material combination, yet since the eigenfrequencies of this model appeared only above 150 kHz, outside of the desired frequency range, this specific material combination will be neglected.

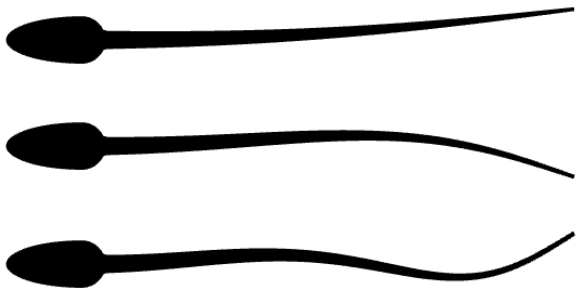

Fig. 2: Mode shapes of the swimmer in the first three eigenfrequencies

As the shell design does not significantly differ in behavior from the solid PDMS swimmer, it will be excluded from the remaining studies. The cavity response shows very different behavior than the other three designs. The peaks are located at higher frequencies and the width of the peaks is smaller. Some resemblance of this behavior can be spotted in the SU8 and Fe solid swimmer responses. The two materials swimmer does not show large differences between the two material combinations, but does differ from the solid design in that its response decays faster with increasing frequency.

3.3 Acoustofluidics

Eigenfrequency evaluation is performed on the two materials PDMS-Fe swimmer. Near the first eigenfrequency (32 kHz) a decrease in elastic energy was found, acoustic radiation force and Stokes drag remained level at an order of 10^{-3}, the LRTT force was found to be of smaller magnitude at 10^{-9}. As this frequency falls outside the desired frequency range, propulsion might not occur, therefore an in depth evaluation will not be performed. The swimmers second eigenfrequency is found at (133 kHz), though this lies within the range of suitable excitation frequencies, due to computational limits it proved difficult to perform simulations above 100 kHz. The cavity design faces the same problem. To make analysis at eigenfrequency possible, the swimmer design has been scaled with a factor of 1.5 in order to shift more

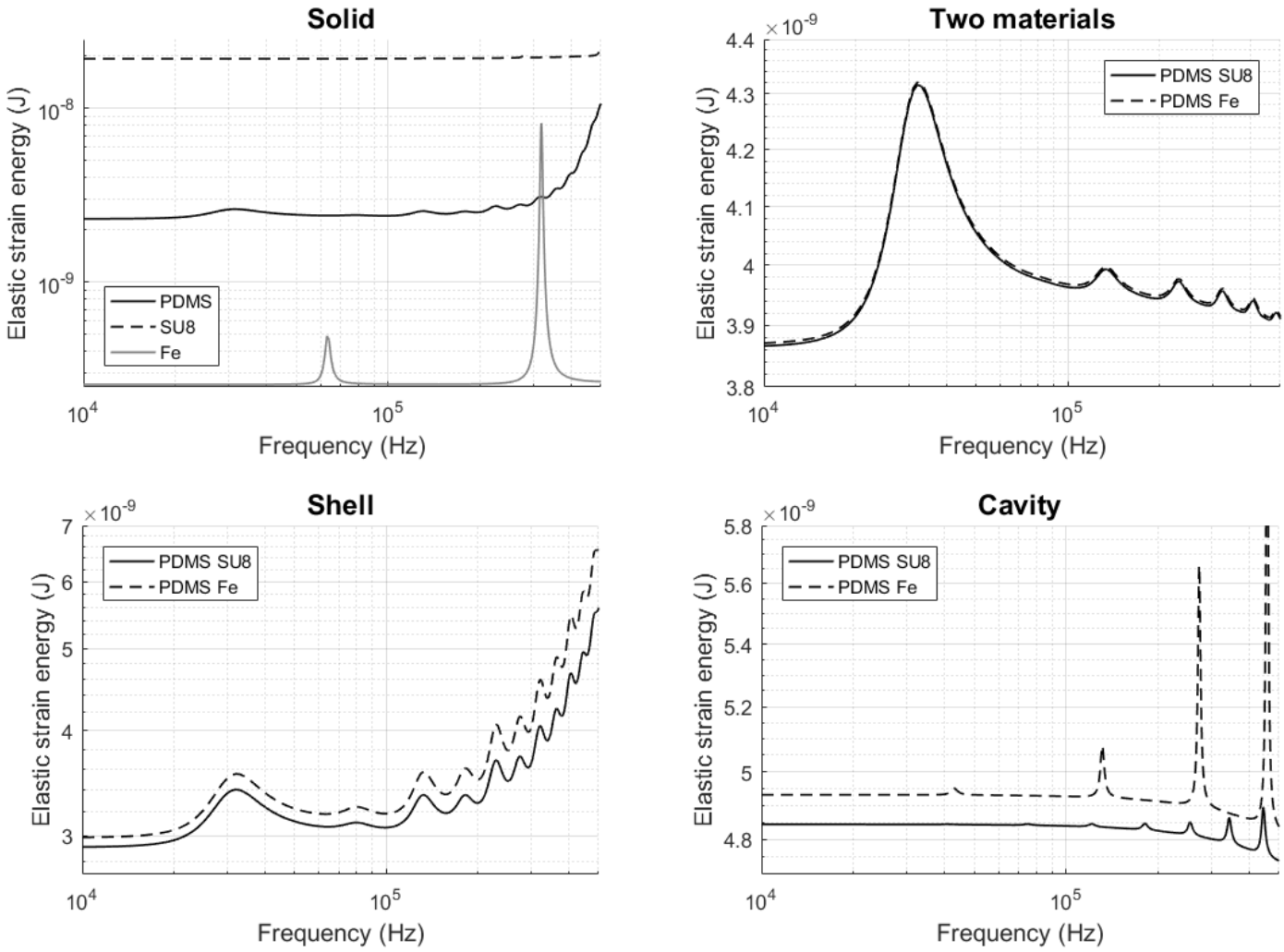

Fig. 3: Elastic strain energy for all swimmer designs

of the higher eigenfrequencies into the suitable excitation range. The new eigenfrequency response can be found in figure 4.

For both models the second eigenfrequency now falls within the computationally viable range. The propulsive force analysis of the two materials and cavity PDMS-Fe scaled swimmers is presented in figure 5. The elastic strain energy peak has shifted somewhat from the eigenfrequency values obtained earlier. For the cavity swimmer differences are observed in the acoustic radiation force and the Stokes drag. These lead to an increase of the total propulsive force around 97 kHz. All propulsive forces have negative values as the swimmer faces the origin, while the x-direction is defined as positive to the right.

The streaming patterns of the fluid are captured at those frequencies where the elastic strain energy is maximum. Alongside with the streaming patterns, a graphical representation of the acoustic radiation

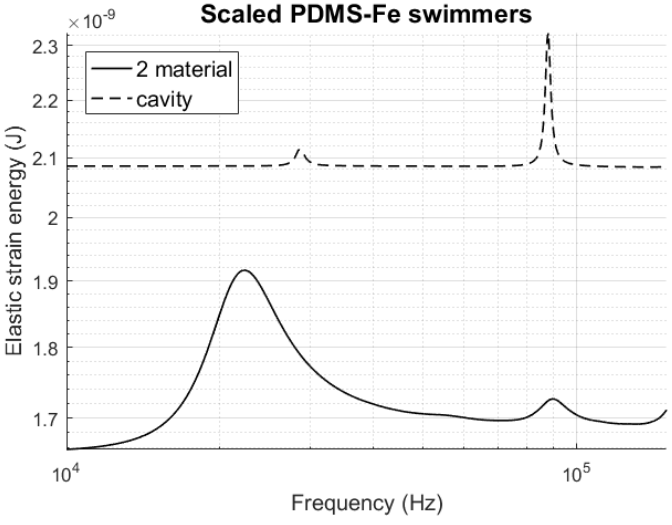

Fig. 4: Frequency response of scaled PDMS-Fe 2mat and cavity swimmers

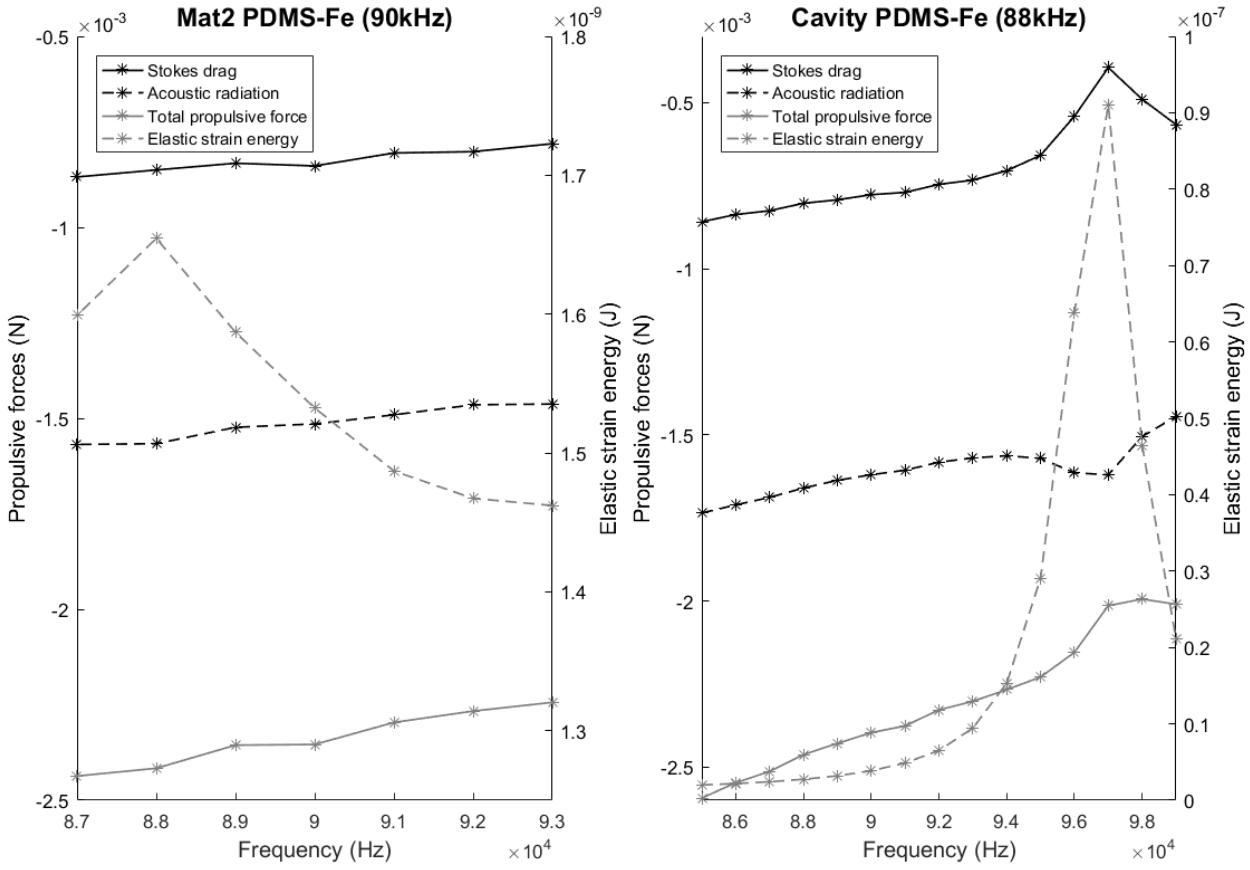

Fig. 5: Propulsive forces for scaled PDMS-Fe 2mat and cavity swimmers at the second eigenfrequency

force and the Stokes drag was recorded. Both can be found in figure 6. For the two materials swimmer the streaming pattern is nearly symmetric over the horizontal, yet it is apparent that more streaming is present at the tip of the tail than over the tail length. An increase in fluid velocity, though smaller, is also visible at the tip of the head and at the connection of head and tail. This is also visible in the image containing the acoustic radiation force and Stokes drag: at the locations mentioned, forces appear on the swimmer surface. The streaming pattern is much more erratic for the cavity swimmer. Fluid velocity is similar at the tip of the head and tail as with the two materials swimmer, yet the forces acting on the surface have increased in magnitude.

The analysis of propulsive forces at 10, 50, 75 and 100 kHz is performed on the original length swimmers. However due to the large stepping size, little variation in propulsion was found and no further analysis is undertaken.

4 DISCUSSION

Structural analysis showed that varying the material composition of the swimmer, caused the eigenfrequencies of the swimmer to shift. An increase in material density caused an increase in eigenfrequency and depending on the amount of contrasting material present, the increase varied. No noticeable influence on the mode shapes was found.

With acoustic excitation the eigenfrequencies of all models shifted to lower values, this is likely to be caused by the extra load the surrounding medium places on the swimmer. Apart from the swimmer itself, the fluid immediately surrounding it must now also be displaced, which causes the resonance frequency to lower [19]. The cavity design had the largest shift in eigenfrequency compared with the original solid design. This might be explained by the large amount of denser material in the tail which causes stiff behavior in the swimmer. The shell design swimmer showed behavior similar to that of the solid PDMS swimmer, apparently a certain amount of

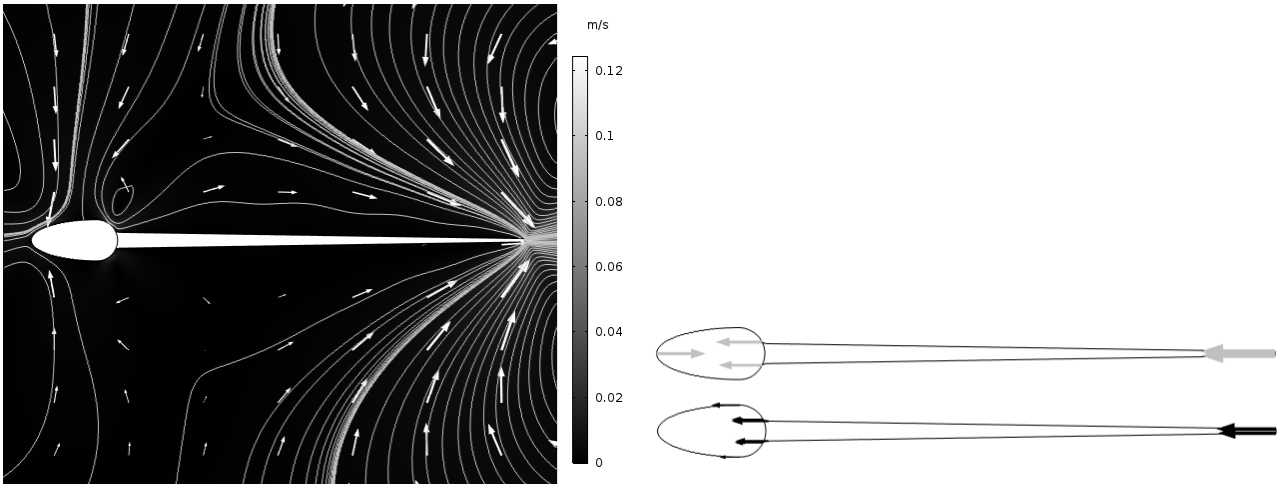

(a) Two material swimmer

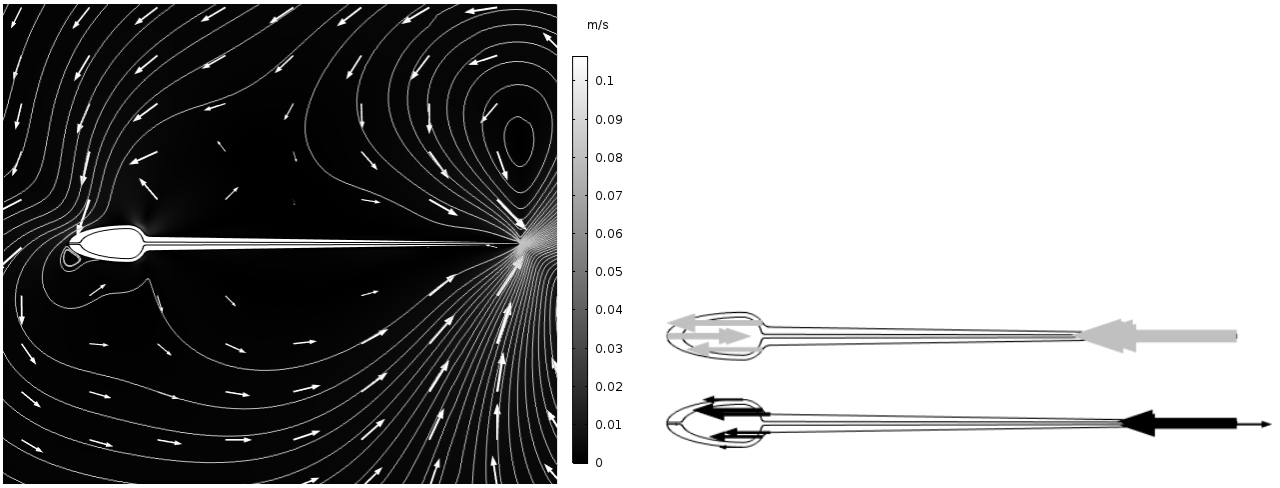

(b) Cavity swimmer

Fig. 6: Streaming patterns around the swimmer and acoustic radiation force (gray) and Stokes drag (black) acting on the swimmer

contrasting material must be present for the response to significantly differ. As the eigenfrequencies of the two materials design, which has more contrasting material than the shell design, were slightly shifted with respect to the solid design, this seems a reasonable explanation. In future investigation experimentation with more materials might be insightful. A larger impact of material variation could be created by adding new material in specific locations of interest, such as the tip of the head or tail of the swimmer.

The thermo-viscous study showed that the swimmers had eigenfrequencies that either fell just inside or largely outside of the 50-100 kHz range. Further means might be taken to shift the eigenfrequencies to more desired locations. Increasing the size of the swimmer is one option, another would be to increase the density of the materials the swimmer is composed of. As can be seen in table 1, the solid iron swimmer has much higher eigenfrequencies than the solid PDMS swimmer. A shift in eigenfrequencies would enable a more detailed study on the propulsive forces. Evaluation of the propulsive forces of the scaled swimmers at eigenfrequency showed very different results between the two designs, as visible in figure 6. The two materials swimmer showed a relatively low maximum in elastic strain energy and little variation can be observed in the acoustic radiation force and Stokes drag. As the excitation occurs at the second eigenfrequency it could be that the swimmers motion is too large to result into large propulsion in the x-direction. The cavity model shows behavior similar to that found by Ahmed et al. [6], at a maximum of the elastic strain energy there occurs a maximum in propulsive forces. At this instance the acoustic radiation force increases, while Stokes drag decreases. The different responses might be explained by the

higher density of the cavity model, which could restrict the motion of the swimmer through the medium and therefore result in a larger amount of propulsion.
From both swimmer designs it is visible in the force images that the Stokes drag increases at the locations were the streamlines come closer to each other. As mentioned in the governing equations section, the Stokes drag is caused by the second order streaming velocity, such that at locations were this velocity increases the Stokes drag increases also. From the left-hand images of figure 6, it can be seen that this occurs near the head and at the tip of the tail. The acoustic radiation force is dependent on the pressure distribution and is most visible at those locations were two vortices meet. At these regions of low pressure the acoustic radiation force will increase and aid to the propulsion of the swimmer. Due to the small number of studies performed it is difficult to extrapolate these results. To do so, further research must be performed at different eigenfrequencies.
As observed in the evaluation at the eigenfrequencies of the cavity and two materials swimmers the propulsive force varied with a kHz step size. Future research would prove most useful when focused at a small frequency range around the eigenfrequencies of the swimmers.

5 CONCLUSION

The structural and acoustics simulations show that it is possible to induce a biological swimming mechanism in a micro-swimmer by mechanical and acoustic excitation. Acoustic actuation of a surrounding medium proved to induce the same response in the swimmer as a mechanical harmonic boundary load exerted on the surface of the swimmer. These eigenfrequency studies indicated the points at which an evaluation of propulsive forces might prove most effective.
Propulsive force evaluation showed that at eigenfrequency the swimmer achieves maximum propulsion. The second orders effects, acoustic radiation force and the Stokes drag, combine with the vibrational response of the swimmer and enhance each other. Perturbation effectively decouples the different timescales in order to solve the non-linear Navier-Stokes and continuity equations. A computational model was constructed, with the use of this decoupling, to evaluate the steady state forces at any desired frequency.
From the proposed designs evaluation at the second eigenfrequency gave indeterminate results, higher eigenfrequencies could be more suitable for further insight. In future studies experiments could be undertaken with by adding contrasting materials in specific locations to fine-tune the influence of material inhomogeneity.

REFERENCES

1. E.M. Purcell. Life at low Reynolds number. *American Journal of Physics*, 45(1):3–11, 1 1977.
2. S. Palagi, D. Walker, T. Qiu, and P. Fischer. Chapter 8 - Micro- and nanorobots in Newtonian and biological viscoelastic fluids. In Minjun Kim, Anak Agung Julius, and U Kei Cheang, editors, *Microbiorobotics (Second Edition)*, pages 133–162. Elsevier, Boston, 2017.
3. L. Zhang, J.J. Abbott, L. Dong, B.E. Kratochvil, D. Bell, and B.J. Nelson. Artificial bacterial flagella: Fabrication and magnetic control. *Applied Physics Letters*, 94(6):064107, 2 2009.
4. G. Loget and A. Kuhn. Electric field-induced chemical locomotion of conducting objects. *Nature Communications*, 2:535, 11 2011.
5. F. Petersson, A. Nilsson, C. Holm, H. Jonsson, and T. Laurell. Continuous separation of lipid particles from erythrocytes by means of laminar flow and acoustic standing wave forces. *Lab on a Chip*, 5(1):20–22, 2005.
6. D. Ahmed, T. Baasch, B. Jang, S. Pane, J. Dual, and B.J. Nelson. Artificial Swimmers Propelled by Acoustically Activated Flagella. *Nano Letters*, 16(8):4968–4974, 8 2016.
7. K.J. Rebello. Applications of MEMS in surgery. *Proceedings of the IEEE*, 92(1):43–55, 2004.
8. M. Wiklund. Acoustofluidics 12: Biocompatibility and cell viability in microfluidic acoustic resonators. *Lab on a Chip*, 12(11):2018–2028, 2012.
9. A. Nilsson, F. Petersson, H. Jonsson, and T. Laurell. Acoustic control of suspended particles in micro fluidic chips. *Lab on a Chip*, 4(2):131–135, 2004.
10. D. Ahmed, M. Lu, A. Nourhani, P.E. Lammert, Z. Stratton, H.S. Muddana, V.H. Crespi, and T.J. Huang. Selectively manipulable acoustic-powered microswimmers. *Scientific Reports*, 5:9744, 5 2015.
11. M. Kaynak, A. Ozcelik, A. Nourhani, P.E. Lammert, V.H. Crespi, and T.J. Huang. Acoustic actuation of bioinspired microswimmers. *Lab Chip*, 17(3):395–400, 2017.
12. S. Kim, S. Lee, J. Lee, B.J. Nelson, L. Zhang, and H. Choi. Fabrication and Manipulation of Ciliary Microrobots with Non-reciprocal Magnetic Actuation. *Scientific Reports*, 6:30713, 7 2016.
13. M.A. Zeeshan, R. Grisch, E. Pellicer, K.M. Sivaraman, K.E. Peyer, J. Sort, B. Özkale, M.S. Sakar, B.J. Nelson, and S. Pané. Hybrid Helical Magnetic Microrobots Obtained by 3D Template-Assisted Electrodeposition. *Small*, 10(7):1284–1288, 12 2013.
14. M. Huth, F. Porrati, and O.V. Dobrovolskiy. Focused electron beam induced deposition meets materials science. *Microelectronic Engineering*, 185-186:9–28, 2018.
15. H. Bruus. Acoustofluidics 2: Perturbation theory and ultrasound resonance modes. *Lab on a Chip*, 12(1):20–28, 2012.
16. A. Lamprecht. *Optical Traps for Characterising Acoustically Induced Forces and Torques Acting on Microparticles*. PhD thesis, ETH Zürich, 2017.

17. K.V. Nemani, K.L. Moodie, J.B. Brennick, A. Su, and B. Gimi. In vitro and in vivo evaluation of SU-8 biocompatibility. *Materials Science and Engineering: C*, 33(7):4453–4459, 2013.

18. F. Schneider, J. Draheim, R. Kamberger, and U. Wallrabe. Process and material properties of polydimethylsiloxane (PDMS) for Optical MEMS. *Sensors and Actuators A: Physical*, 151(2):95–99, 2009.

19. M.K. Ghatkesar, T. Braun, V. Barwich, J. Ramseyer, C. Gerber, M. Hegner, and H.P. Lang. Resonating modes of vibrating microcantilevers in liquid. *Applied Physics Letters*, 92(4):043106, 1 2008.

A TABLE WITH SIMULATION PARAMETERS

Some parameters that were not provided by COMSOL are presented in the table below. Scaling factors used in the acoustofluidic model for the traveling soundwave are also provided.

Parameter	Value	Description
$dvisc_0$	$50[um]\sqrt{100[Hz]/f_0}$	Mesh viscous penetration depth at study frequency
λ_0	$c_f/f0$	Wavelength
c_f	1502[m/s]	Fluid speed of sound
ρ_f	1000[kg/mˆ3]	Fluid density
β_{f0}	4.45e-10[1/Pa]	Fluid isentropic compressibility
α_{f0}	2.75e-4[1/K]	Fluid thermal expansion
C_{pf}	4.18e3[J/(kgK)]	Fluid heat capacity at constant pressure
γ_f	1,012	Fluid ratio of specifc heats
μ_f	8.5e-4[Pas]	Fluid dynamic viscosity
μB_f	2.4e-3[Pas]	Fluid bulk viscosity
$kcond_f$	6.1e-1[W/(mK)]	Fluid thermal conduction
Scaling factors for excitation wave		
W_{scaled}	W/(10E-4)	Scaling factor for the width of the domain
f_{scaled}	f0/(10E4)	Scaling factor for the frequency